Acta Crystallographica Section D
Biological Crystallography
ISSN 0907-4449

Structure of DNA helicase RepA in complex with sulfate at 1.95 Å resolution implicates structural changes to an 'open' form

Hai Xu,[a] Norbert Sträter,[a] Werner Schröder,[a] Christoph Böttcher,[b] Kai Ludwig[b] and Wolfram Saenger[a]*

[a]Institut für Kristallographie, Freie Universität Berlin, Takustrasse 6, D-14195 Berlin, Germany, and [b]Forschungszentrum für Elektronenmikroskopie, Freie Universität Berlin, Fabeckstrasse 36a, D-14195 Berlin, Germany

Correspondence e-mail: saenger@chemie.fu-berlin.de

Received 1 November 2002
Accepted 18 February 2003

PDB Reference: RepA–sulfate complex, 1nlf, r1nlfsf.

The structure of a new crystal form (space group *C*2), grown at pH 8.0 and diffracting to 1.95 Å resolution, of the replicative homo-hexameric DNA helicase RepA encoded by plasmid *RSF1010* is reported. In contrast to previous crystals grown at pH 6.0 in space group $P2_1$ (Niedenzu *et al.*, 2001), only one half (a trimer) of the RepA hexamer occupies the asymmetric unit of the space-group *C*2 crystals. The new crystal packing explains the pH-dependent hexamer–hexamer association mechanism of RepA. The C-terminus ^{264}VLERQRKS-KGVPRGEA^{279}, which could not be modelled in the previous structure, is clearly defined in the present electron density except for the last four amino acids. Sulfate anions occupy the six ATPase active sites of RepA at positions where the product phosphates are supposed to bind. Binding of sulfate anions induces conformational changes both at the ATPase active sites and throughout the whole molecular structure. In agreement with electron microscopy, the above studies implicate structural changes to an 'open' form that may occur upon binding and hydrolysis of nucleotide 5′-triphosphates and could be essential for DNA duplex-unwinding activity.

1. Introduction

DNA helicases are a large family of motor proteins with essential roles in key biological processes including DNA replication, transcription, repair and recombination (Matson & Kaiser-Rogers, 1990; Lohman & Bjornson, 1996). They unwind double-stranded DNA (dsDNA) using the chemical energy of nucleoside 5′-triphosphate (NTP) hydrolysis. Malfunction of specific helicases results in human diseases such as Bloom's and Werner's syndromes (Ellis, 1997) and has been associated with the development of cancer (Egelman, 1996) and with aging (Bowles, 1998). All DNA helicases for which the assembly state of the enzyme has been examined appear to function as oligomers, generally dimers or hexamers, thus providing the multiple potential DNA-binding sites that are required for helicase function.

Several high-resolution structures have been reported for monomeric/dimeric helicases. A common helicase architecture has been revealed by crystal structures of two DNA helicases, *Bacillus stearothermophilus* PcrA (Velankar *et al.*, 1999) and *Escherichia coli* Rep (Korolev *et al.*, 1997), and an RNA helicase, the hepatitis C virus NS3 protein (Kim *et al.*, 1998). The recently determined crystal structure of PcrA complexed with a DNA substrate revealed details of the helicase mechanism (Soultanas & Wigley, 2000). For intact unmodified replicative hexameric helicases, information is limited to low-resolution electron-microscopic studies (Patel & Picha, 2000). Crystal structure analyses of truncated domains of two

hexameric helicases, *E. coli* DnaB (Fass *et al.*, 1999) and bacteriophage T7 helicase–primase (Sawaya *et al.*, 1999; Singleton *et al.*, 2000), have been reported. In the structure of the latter, the deviation from expected sixfold symmetry of the hexamer indicates that the structure represents an intermediate on the catalytic pathway, which probably involves structural changes. The structural consequences of the asymmetry suggest a 'binding change' mechanism to explain how cooperative binding and hydrolysis of NTP are coupled with conformational changes in the ring that most likely accompany duplex unwinding.

The replicative hexameric helicase RepA is encoded by the broad host-range plasmid *RSF1010*, an 8684 base pair (bp) multicopy plasmid that is found in a wide variety of Gram-negative and Gram-positive actinomyces (Scholz *et al.*, 1989). RepA belongs to the DnaB-like helicase family and is one of the smallest known hexameric helicases, with 278 amino acids in the monomer. It unwinds DNA in the 5′–3′ direction and *in vitro* biochemical data show that at pH 5.5–6.0 RepA has optimal single-stranded DNA (ssDNA) stimulatable ATPase activity and dsDNA-unwinding activity. At and below this pH range, RepA tends to aggregate as dimers of hexamers and even larger complexes (Scherzinger *et al.*, 1997; Xu, Frank, Holzwarth *et al.*, 2000; Xu *et al.*, 2001). At pH 7.0–8.0, RepA occurs exclusively as homohexamer as shown by ultracentrifugation and fluorescence correlation spectroscopy studies (Xu *et al.*, 2001).

RepA is the first intact hexameric replicative DNA helicase for which the three-dimensional structure has been determined (Niedenzu *et al.*, 2001). The RepA hexamer shows a cone-shaped annular structure with sixfold rotational symmetry and a 17 Å wide central hole, suggesting that ssDNA but not dsDNA can pass through the central channel during unwinding. Homologues of all five conserved sequence motifs of the DnaB-like helicase family are found in RepA; in a modelled ATP–RepA complex, the six ATP-binding sites of RepA are each located at the interfaces between two adjacent monomers (Niedenzu *et al.*, 2001). They comprise the conserved Walker A and B motifs that are defined by the consensus sequence ^{40}GAGKS^{44} for the P-loop (Saraste *et al.*, 1990) and by Glu77, Asp140, His179 (belonging to the same

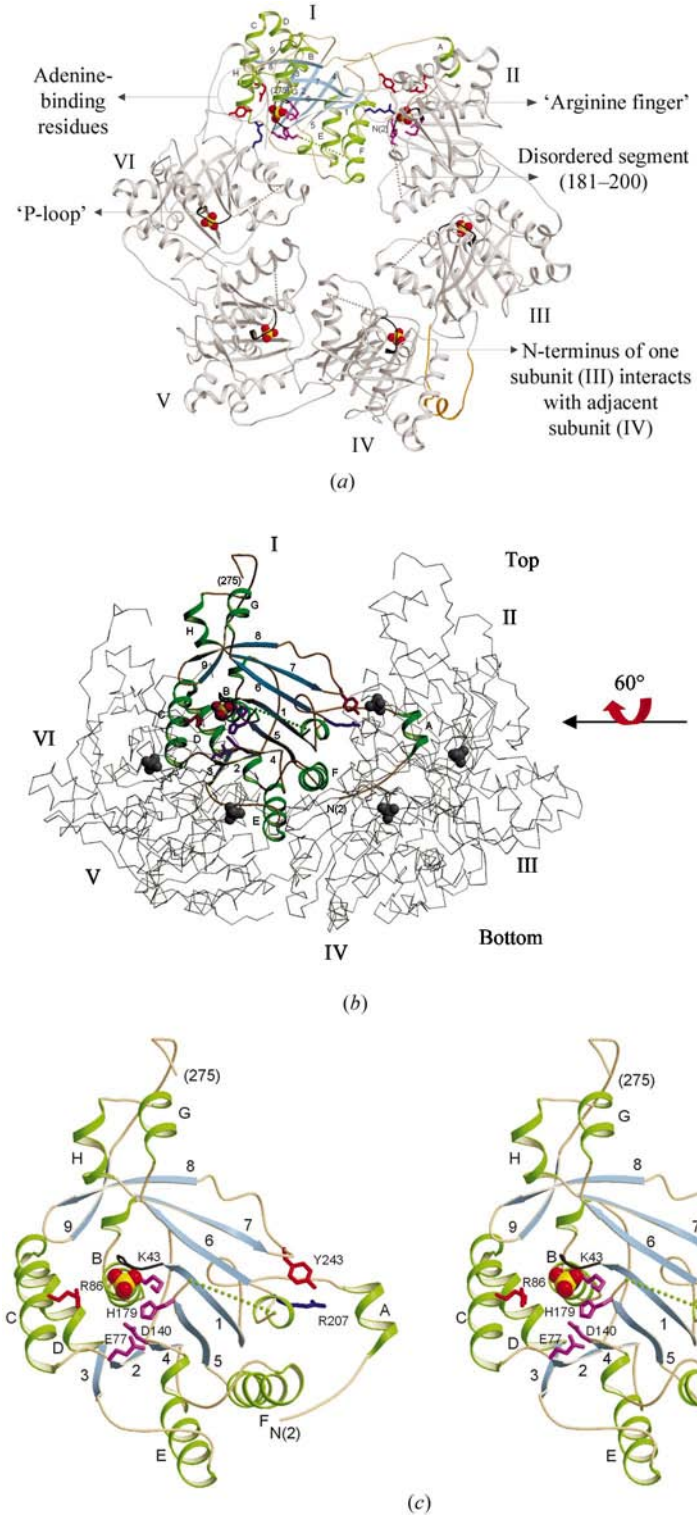

Figure 1
(*a*) View of the RepA homohexamer from the 'top'. Each monomer is marked with Roman numbers. In subunit I (see also Fig. 1*c*), α-helices *A*–*H* and β-strands 1–9 are labelled. SO_4^{2-} anions (red O atoms) are shown in the active sites. The adenine-binding residues (red), 'arginine finger' (blue), other active-site residues (purple), 'P-loop' (black), disordered segment (dotted line) and the interaction of the N-terminus of one subunit with the adjacent one (yellow) are marked (for details, see Niedenzu *et al.*, 2001). (*b*) The molecule shown in Fig. 1(*a*) was rotated exactly 60° about the *x* axis (horizontal) to show the 'top' and 'bottom' of RepA. Monomer I is outlined and labelled; the other monomers are shown as a C^{α} trace. (*c*) Stereoview of the RepA monomer (same orientation as monomer I shown in Fig. 1*b*). β-Strands are blue and labelled with numbers; α-helices are green and labelled with capital letters. The C-terminus beyond Pro275 could not be modelled; the disordered segment (181–200) is indicated by the green dotted line. All figures except Fig. 5 were prepared with *MOLSCRIPT* (Kraulis, 1991) and rendered using *RASTER3D* (Merritt & Bacon, 1997).

monomer) and the 'arginine finger' Arg207 from the adjacent monomer, respectively (these amino acids are indicated in Fig. 1). Similar to the helicase domain of the bacteriophage T7 gp4 protein (Sawaya *et al.*, 1999), the 'arginine finger' Arg207 contributes to the active site and suggests cooperativity between monomers in the ATP hydrolysis and helicase activity of RepA. The adenine base of ATP is found sandwiched between Arg86 of the same (*cis*) and Tyr243 of the adjacent (*trans*) monomer (Niedenzu *et al.*, 2001).

The previous crystals grew at pH 6.0 in space group $P2_1$. They diffracted to 2.4 Å resolution and in the asymmetric unit two cone-shaped hexamers are stacked in a bottom-to-bottom orientation. Both the loop ^{181}SKGAAMMGAGDQQQ-ASRGSS^{200} connecting β-strands $\beta5$ and $\beta6$ and the C-terminus ^{264}VLERQRKSKGVPRGEA^{279} are disordered and could not be modelled owing to poorly defined electron density. Here, we report a new crystal form of RepA, space group $C2$, which grows at pH 8.0 and diffracts to a resolution of 1.95 Å. This new structure clearly defines the C-terminus which is involved in intermolecular interactions; the ATP-binding sites are all occupied by sulfates that appear to induce a series of structural changes.

2. Materials and methods

2.1. Protein expression, purification and crystallization

RepA protein was prepared using an overproducing strain of *E. coli* (Scherzinger *et al.*, 1991) and purified at 277 K as described in Röleke *et al.* (1997). Crystals were grown by vapour diffusion employing the hanging-drop technique at 291 K. 3 µl of protein solution (17 mg ml^{-1}) in a buffer containing 40 m*M* 4-morpholinethanesulfonic acid (MES)/NaOH pH 5.8, 10 m*M* $MgCl_2$, 80 m*M* NaCl plus 100 µ*M* $(dT)_{12}$ and 1 m*M* β,γ-imidoadenosine 5′-triphosphate (AMP-PNP) were mixed with 3 µl reservoir solution consisting of 28% PEG 4000, 200 m*M* $MgSO_4$ and 100 m*M* Tris–HCl pH 8.0. Within one week, needle-shaped crystals of dimensions 2.0 × 0.05 × 0.05 mm were obtained. Although the X-ray structure analysis showed no binding of $(dT)_{12}$ and AMP-PNP in the final structure, they have a favourable influence on crystal growth; without these additions, RepA does not form crystals under the same conditions.

2.2. X-ray data collection

Single crystals were cut to dimensions of 0.5 × 0.05 × 0.05 mm and flash-cooled (100 K) in a rayon loop using the reservoir solution plus 15% glycerol as cryoprotectant. X-ray diffraction data were collected at the BESSY II synchrotron (Berlin) using a MAR 345 image plate. The data were integrated and processed with *DENZO* and *SCALEPACK* (Otwinowski & Minor, 1997). Crystallographic data and refinement statistics are given in Table 1.

2.3. Structure determination and refinement

The structure was determined by molecular replacement on the basis of the 2.4 Å resolution model of RepA (Niedenzu *et al.*, 2001) using the *AMoRe* program (Navaza, 1994). The volume of the unit cell suggested the presence of a trimer (half a hexamer) in the crystal asymmetric unit, yielding a Matthews coefficient of 2.62 Å^3 Da^{-1} (Matthews, 1968). Consequently, half the RepA hexamer was used as a search model, yielding one solution that was clearly better than any other, with correlation coefficients of 53.2% (Corr_F), 58.8% (Corr_I) and an R factor of 47.0% for data in the resolution range 87.7–4.0 Å. The model was subjected to rigid-body refinement using *CNS* (Brünger *et al.*, 1998) for data in the resolution range 20–1.95 Å, converging at an R value of 35.9% for all data and an $R_{\rm free}$ value of 36.2% for 5% of the data (Brünger, 1992, 1993). The model was improved by simulated annealing followed by energy minimization and B-value refinement with *CNS*. For manual rebuilding, the computer graphics package *O* (Jones *et al.*, 1991) was used. Three sulfate anions and 756 water molecules were added in the $F_o - F_c$ difference electron-density map at peaks 3 r.m.s. deviation above mean density and within hydrogen-bonding distances of protein atoms or other water molecules. The refinement converged at R = 20.1% and $R_{\rm free}$ = 24.2%, with an average temperature factor of 21.4 Å^2. Further refinement details are given in Table 1.

Table 1
Data-collection and refinement statistics.

Values in parentheses are for the outermost resolution shell.

Data collection	
Space group	*C*2
Unit-cell parameters (Å, °)	a = 192.3, b = 55.3, c = 105.6, β = 122.9
Resolution (Å)	20.0–1.95
Total observations	243785
Unique observations	72794
$R_{\rm sym}$†	0.078 (0.097)
$I/\sigma(I)$	9.1 (6.8)
Completeness (%)	98.4 (99.6)
Model refinement	
$R_{\rm cryst}/R_{\rm free}$‡	0.201/0.242
Resolution range (Å)	20.0–1.95
R.m.s. deviations from stereochemical target values	
Bond lengths (Å)	0.005
Bond angles (°)	1.23
Average B values (Å^2)	
All atoms	21.4
Protein main chains	16.9
Protein side chains	24.6
Water molecules and sulfates	28.1
Ramachandran plot§	
Residues in most favoured region (%)	91.5
Residues in additionally allowed region (%)	8.5

† $R_{\rm sym} = \sum|I - \langle I\rangle|/\sum I$, where $\langle I\rangle$ is the average intensity over symmetry-equivalent reflections. ‡ $R_{\rm cryst}$ and $R_{\rm free} = \sum||F_o| - |F_c||/\sum|F_o|$, where F_o and F_c are the observed and calculated structure-factor amplitudes. For the calculation of $R_{\rm free}$, 5% of the reflection data were selected in thin resolution shells and omitted from refinement. § As defined by *PROCHECK* (Laskowski *et al.*, 1993).

2.4. Electron microscopy and three-dimensional reconstruction

2.4.1. Electron microscopy. For electron-microscopy investigations (cryo-TEM) and the subsequent three-dimensional reconstruction, 10 µ*M* RepA protein (monomer)

was prepared in 40 m*M* MES buffer solution pH 5.8 in the presence of 10 m*M* $MgCl_2$, 60 m*M* NaCl and 1 m*M* adenosine-5′-*O*-(3-thiotriphosphate) (ATPγS). Droplets of the sample (5 µl) were applied to hydrophilized [glow discharge in a BALTEC MED 020 (BAL-TEC AG, Liechtenstein) for 60 s at 8 W] carbon-covered microscopical copper grids (400 mesh) and supernatant fluid was removed with a filter paper until an ultrathin layer of the sample was obtained. A droplet of contrasting material (2% phosphotungstic acid) was added and blotted. A heavy-metal-stained layer of the protein assemblies was thus prepared and subsequently plunged into liquid ethane for vitrification in order to preserve the protein structure in its fully hydrated state. A Gatan-626 specimen holder/cryotransfer system was used in a Philips Tecnai F20 FEG TEM (FEI Company, Oregon), keeping the sample at a constant temperature of 94 K. Imaging was performed under low-dose conditions using a primary magnification of 61 702× at an accelerating voltage of 160 kV. The defocus value was chosen to correspond to a first zero of the CTF at ∼12 Å. This specimen-preparation procedure was essentially the same as that described previously for the three-dimensional structure determination of influenza HA (Böttcher *et al.*, 1999). The embedding matrix used has a somewhat higher contrast compared with the conventional vitreous-ice preparation and allows the localization of single molecules despite the relatively high acceleration voltage of the microscope and the chosen 'close-to-focus' imaging conditions.

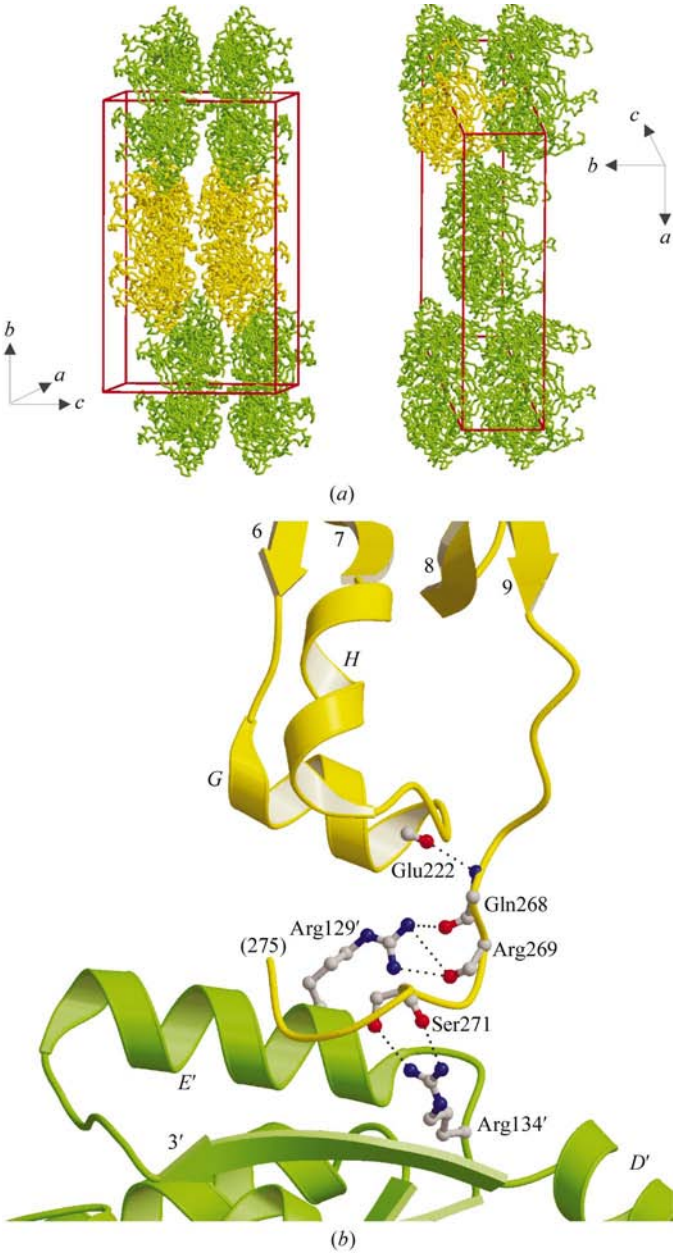

Figure 2
(*a*) Different views of RepA crystal packing in space group $P2_1$ (left) and space group *C*2 (right). In space group $P2_1$ two RepA hexamers in bottom-to-bottom orientation (yellow) occupy the asymmetric unit; in contrast, one half of the RepA hexamer (yellow) occupies the asymmetric unit in space group *C*2 (right) and RepA hexamers are oriented top-to-bottom. (*b*) Intermolecular crystal contacts between C-terminal residues (to Pro275; the four additional C-terminal amino acids were not traceable in the electron density) of one RepA (yellow) and the helix $\alpha E'$ of the adjacent RepA molecule (green). Hydrogen bonds are indicated by dotted lines.

2.4.2. Reconstruction of the three-dimensional structure. Laser-light diffraction by electron micrographs was employed to select 'good' micrographs in terms of optically correct phase-contrast transfer (absence of aberration, drift, astigmatism *etc.*). The selected micrographs were digitized using a Primescan drum scanner (Heidelberger Druckmaschinen AG, Heidelberg, Germany) at a pixel resolution of 0.68 Å in the digitized images. All image processing was performed using the *Imagic*-5 software package (van Heel *et al.*, 1996) under the Linux operating system. 6134 molecules were interactively selected and extracted from the digitized micrographs as 400 × 400 pixel fields. For computational efficiency, these single images were interpolated to 1.36 Å pixel size for all subsequent steps. Using the angular reconstitution technique (van Heel, 1987), Euler angles were *a posteriori* assigned under *D*6 symmetry restraint and a first rough three-dimensional reconstruction was calculated. Refinements were performed in an iterative process by using forward projections of the preliminary reconstruction as an 'anchor set' for consecutive steps. Fourier shell correlation (FSC; van Heel & Harauz, 1986) of two different three-dimensional reconstructions, each of which included half of the final class averages, was performed to assess the resolution. The 3σ threshold criterion curve was then corrected by a factor of 12 to account for the assumed *D*6 point-group symmetry (Orlova *et al.*, 1997). For both three-dimensional structures, the resolution obtained in the final three-dimensional reconstruction was determined to be ∼16.5 Å. Three-dimensional alignment of X-ray data of RepA (PDB ID 1g8y) and TEM data was performed using the *AMIRA* 2.3 software.

3. Results

3.1. Quality of the model

RepA crystallizes in space group *C*2 with half a hexamer (a trimer) in the asymmetric unit. In the present model, the

C-terminal residues ^{264}VLERQRKSKGVPRGEA^{279}, which could not be modelled previously (Niedenzu *et al.*, 2001), were clearly traceable in the present electron density to Pro275 and were included in the final model (Fig. 1). However, the segment ^{181}SKGAAMMGAGDQQQASRGSS^{200} is still not defined in the electron density and was omitted from the final model. Each of the three RepA monomers contains one sulfate anion ($MgSO_4$ was present in the crystallization buffer) and a total of 756 water molecules are bound to the trimer. The mean atomic coordinate error according to Luzzati (1952) is less than 0.25 Å. The Ramachandran plot calculated using *PROCHECK* (Laskowski *et al.*, 1993) showed 91.5% of the residues in the most favoured regions and the remaining 8.5% in additionally allowed regions. The average temperature factor is 16.9 Å^2 for the main-chain atoms, 24.6 Å^2 for the side-chain atoms and 28.1 Å^2 for water molecules and sulfate anions (see Table 1).

3.2. General description of the structure

The previous crystals (Niedenzu *et al.*, 2001) were grown at pH 6.0 and in the crystal lattice (space group $P2_1$) the cone-shaped hexamers are stacked in a bottom-to-bottom orientation along the crystallographic *c* axis to form dihexamers (Fig. 2*a*). The crystals described here grew at pH 8.0 in space group *C*2, which has no resemblance to the former $P2_1$ and has a much smaller asymmetric unit containing only one half of the RepA hexamer. The packing of the RepA hexamer in the *C*2 crystal form is depicted in Fig. 2(*a*). The sixfold symmetry axis of the hexamer coincides with the crystallographic twofold rotation axis parallel to *b* and the hexamers are stacked top-to-bottom along the *b* axis.

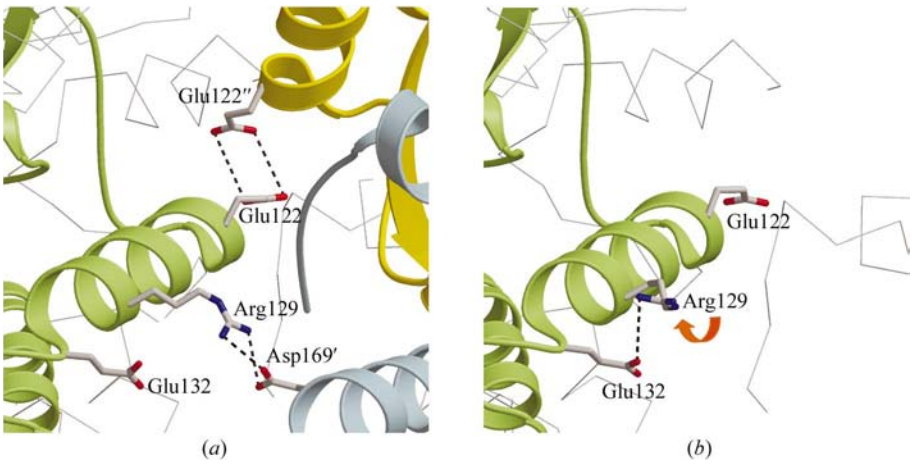

Figure 3
(*a*) View of a section showing the interface interactions between two RepA hexamers stacked 'bottom-to-bottom' at pH 6.0 (space group $P2_1$). The residues shown of one subunit (green) from one hexamer are hydrogen bonded to two subunits (yellow and blue) from the other hexamer. A total of six such interactions exist at the interface between the two hexamers. (*b*) In the crystal structure at neutral pH (space group *C*2), Arg129 bends towards and is hydrogen bonded to Glu132 from the same molecule (intramolecular); by contrast, at pH 6.0 the side chain of Arg129 is more extended and forms hydrogen bonds with Asp169′ of the adjacent hexamer (intermolecular) (Fig. 3*a*).

3.3. pH-dependent hexamer–dihexamer equilibrium

In the previous $P2_1$ crystal structure obtained at pH 6.0, the two cone-shaped RepA hexamers in the dihexamer forming the asymmetric unit are rotated with respect to each other by $\sim30^\circ$ about the common sixfold rotation axis so that the α-helices αE that protrude from the 'bottom' side of the cone (Fig. 1*b*) can interdigitate and stabilize the dodecamer structure. At the hexamer–hexamer interface of RepA, the side chains of Asp169 and Arg129 from each subunit of one hexamer are hydrogen bonded to Arg129′ and Asp169′ of the other hexamer, respectively (Fig. 3*a*), and hydrogen bonds are formed between Glu122 and Glu122′ of adjacent subunits in the dihexamer, *i.e.* Glu122 $O^{\varepsilon1}\cdots$Glu122′ $O^{\varepsilon2}$ and Glu122 $O^{\varepsilon2}\cdots$Glu122′ $O^{\varepsilon1}$. At pH 6.0, these two Glu122 carboxylates in RepA are likely to be protonated and to allow inter-subunit hydrogen bonding between the Glu122 and Glu122′ carboxyl groups and stabilization of the dihexamer. At neutral pH, Glu122 will be deprotonated and the association of the two hexamers is destabilized because the negatively charged Glu122 and Glu122′ side chains repel each other. A comparable albeit different pH-dependent dimer–octamer equilibrium in arylsulfatase A has been proposed to be caused by deprotonation–protonation of carboxylate or imidazole side chains (Nichol & Roy, 1966; Nicholls & Roy, 1971; Lukatela *et al.*, 1998; Vagedes *et al.*, 2002).

In the crystal form described here, which grows at pH 8.0, the RepA hexamers are not stacked bottom-to-bottom. This is because the negatively charged Glu122 side chains can no longer form Glu122$\cdots$Glu122′ hydrogen bonds and, in addition, the Arg129 residues at the 'bottom' of RepA are now rotated towards and hydrogen bonded to Glu132 residues from the same subunit (intramolecular) and are consequently located far away from their position at acidic pH (Figs. 3*a* and 3*b*). This explains why only hexamers were observed by analytical ultracentrifugation in solution under neutral pH 7.6 conditions, while at acidic pH RepA tends to aggregate as dihexamers (dodecamers) and higher forms (Xu, Frank, Holzwarth *et al.*, 2000).

3.4. Crystal packing and intermolecular interactions

Since solvent occupies only 33% of the crystal volume in the *C*2 crystal form, the packing of the RepA molecules is relatively tight. The C-termini of each hexamer form intermolecular top-to-bottom contacts with the adjacent hexamer translated along the *b* axis (Fig. 2*b*). This explains why in this crystal packing most of the flexible C-terminus is well defined (the last four amino acids are still dis-

ordered), in contrast to the $P2_1$ crystal form where the C-termini from adjacent hexamers face each other and are disordered from Val264 onwards.

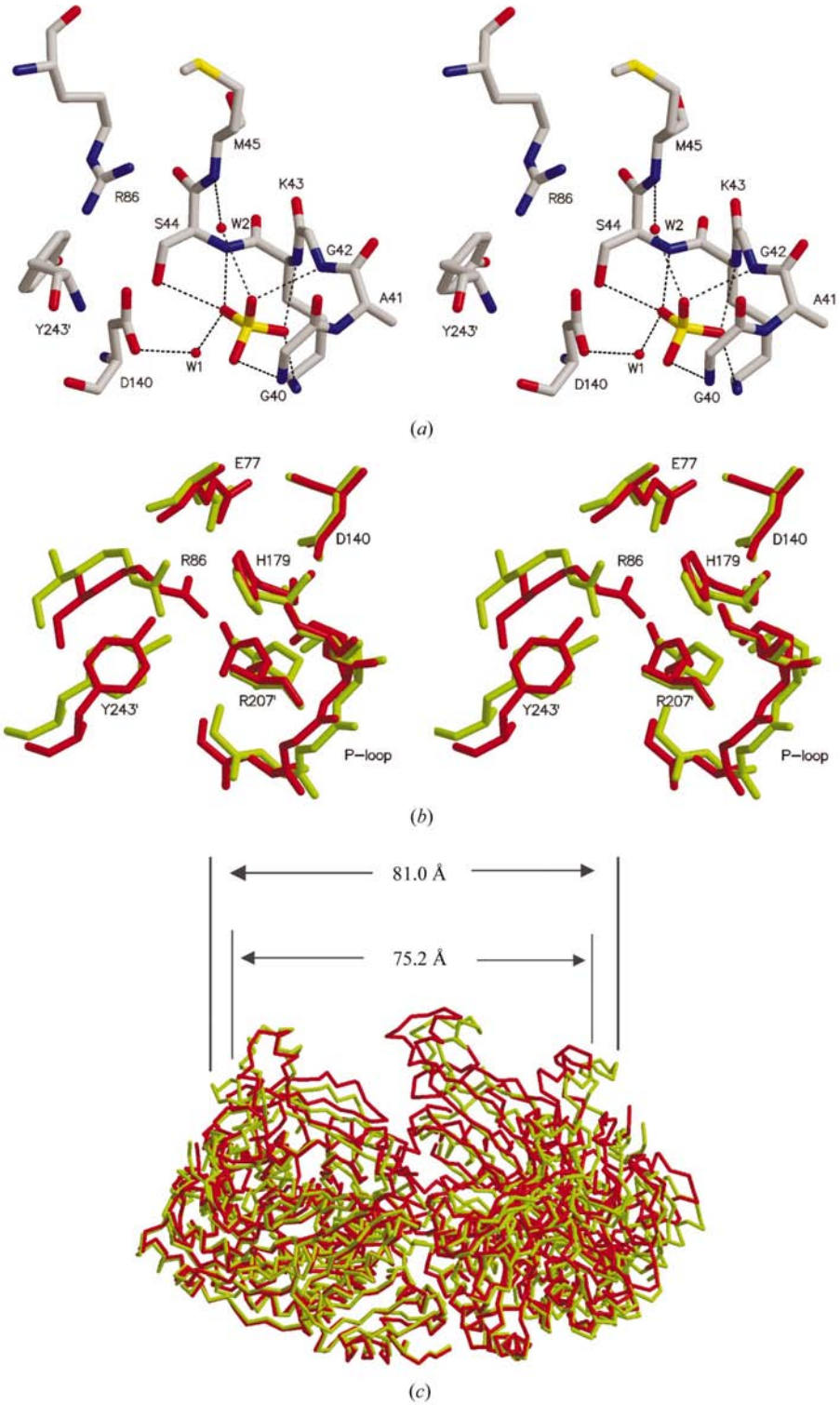

Figure 4
Stereoview of the ATPase active site. (*a*) Active site showing the interaction of sulfate anion and P-loop residues. (*b*) Superimposition of the active sites of the free RepA hexamer structure ($P2_1$, red) and sulfate-liganded RepA hexamer ($C2$, green). (*c*) Superimposition of the two structures of RepA hexamers, colour coding as in (*b*). Distances between equivalent positions across the hexamers are indicated by double-headed arrows.

In the $C2$ crystal form of RepA, amino-acid residues at the C-terminus (266–275) close to the 'top' of the cone are mainly linked with amino-acid residues 107–134 at the 'bottom' of the adjacent molecule through a number of hydrogen bonds, and hydrophobic contacts are formed between main-chain and side-chain groups. Gln268 O and Arg269 O each accept a hydrogen bond from the guanidinium group of Arg129′ of the adjacent molecule; Ser271 O and O^{γ} form hydrogen bonds to Arg134′ $N^{\eta 2}$ and $N^{\eta 1}$, respectively (Fig. 2*b*). The C-terminal residues 269–275 form a cluster of hydrophobic interactions with side chains of Pro70′ and Leu74′ at β2, Leu107′ and Gln109′ at β3, and Trp123′, Gly126′, Pro129′ and Ala130′ at αE from the adjacent *b*-translation-related RepA (data not shown).

3.5. Binding of sulfate at ATPase active sites induces conformational changes

In this crystal structure, none of the six ATPase active sites of RepA is occupied by AMP-PNP, which was added to the crystallization buffer, but sulfate anions are clearly seen in the difference electron density at the putative binding site for the nucleotide phosphate. The 'P-loop' segment Gly40–Ser44 (Walker A motif) of RepA connnecting β1 and αB forms a pocket that accommodates the sulfate anion. Besides interacting with the 'P-loop', the sulfate is also hydrogen bonded to the conserved residue Asp140 from the Walker B motif *via* water molecules (Fig. 4*a* and Table 2). The conserved Lys43 on the 'P-loop' is functionally essential since the mutant Lys43Ala has nearly no ATPase activity and only weak binding affinity for ATP (E. Lanka, H. Xu & G. Ziegelin, unpublished data).

The 'P-loop' is better ordered in the sulfate-bound RepA compared with the unliganded enzyme (Niedenzu *et al.*, 2001). This is evidenced in the present structure by the average temperature factor (*B* value), which is 13.7 Å^2 for this loop (20.9 Å^2 for the whole structure) and 44.1 Å^2 (46.3 Å^2 for the whole structure) in free RepA.

When superimposing the active site from the present structure with that

from the $P2_1$ crystal grown at pH 6.0 in which the nucleotide-binding sites are empty, the C^{α} r.m.s. deviation is 1.1 Å and some regions deviate more strongly than others. In particular, residues Arg86, Gly40 (beginning of the P-loop) and the 'arginine finger' Arg207′ (from the adjacent monomer) diverge greatly (see Fig. 4*b*). Notably, the main-chain conformation of the Walker motif A is not affected.

The r.m.s. deviation increases to 1.82 Å between C^{α} positions when the whole RepA hexamers are superimposed, suggesting that the two structures differ to some extent. In the sulfate-bound structure the 'top' part of the hexamer (the narrower side of the cone; Fig. 1*b*) is 'opened up' from 75.2 to 81.0 Å (in diameter when looking along the pseudo-C_6 axis), involving mainly helix αG and the C-terminal residues. The shape of the 'bottom' (the wider side of the cone) of the hexamer is nearly the same (Fig. 4*c*) and no significant deviations from the sixfold symmetry are seen here in both structures.

3.6. Electron-microscopic studies of conformational changes induced by ATPγS binding

Similar results were also obtained using electron microscopy to study ATPγS binding to RepA. In the presence of ATPγS at pH 5.8, electron micrographs show that upon binding of the non-hydrolyzable ATP analogue ATPγS, RepA changes its structure compared with the X-ray structure of free RepA crystallized at pH 6.0, but dihexamers stacked bottom-to-bottom are also found in EM studies (Fig. 5). When superimposing the free RepA structure (pH 6.0; Niedenzu *et al.*, 2001) with the three-dimensionally reconstructed EM images, we found similar results as shown in Fig. 4(*c*): the main conformational changes also occur at the 'top' parts of the RepA hexamer. Upon binding of ATPγS, the RepA hexamer is in an 'open' form compared with the 'closed' form of the non-liganded RepA, especially around helix αG and the C-terminal region at the 'top' of the cone. The 'bottom' parts remain nearly the same.

4. Conclusions

In the helicase domain of bacteriophage T7 (Sawaya *et al.*, 1999), residues 554–566 comprise the acidic C-terminal tail that is critical for the physical interaction with T7 DNA polymerase during replication. This protein–protein interaction, which is required for phage growth, was shown to coordinate DNA-unwinding activity with the synthesis of the leading strand of the replication fork (Notarnicola *et al.*, 1997). In the crystal structure of bacteriophage T7, this C-terminal segment could not be modelled with certainty (probably owing to disorder) and was not included in the final model. In RepA, the C-terminus is important *in vivo* since deletion of certain amino acids of the C-terminus can lead to cell death (E. Lanka & G. Ziegelin, personal communication). In both RepA crystal structures, space groups $P2_1$ and $C2$, the segment ^{181}SKGAAMMGAGDQQQASRGSS^{200} is found to be disordered. As outlined in Niedenzu *et al.* (2001), this suggests that the disorder is of functional importance, especially since the tripeptide ^{197}RGS^{199}, which is part of this segment, was shown to be engaged in DNA binding (E. Lanka & G. Ziegelin, personal communication).

Many attempts to co-crystallize RepA with standard NDP or with non-hydrolyzable NTP analogues and to soak RepA crystals with solutions containing these analogues have so far failed. These experiments always resulted in partially low-occupied nucleotide-binding sites, making unambiguous definition of inhibitor binding impossible. In the present crystal structure, sulfate anions occupy positions in the RepA hexamer where the product phosphate groups should be

Table 2
Hydrogen-bonding of ATPase active-site residues with the sulfate anion.

Sulfate or water	Hydrogen-bonded group	Distance (Å)
O1	Gly40 N	2.83
O2	Gly42 N	2.94
	Ow2	3.03
O3	Lys43 N^{ζ}	2.78
	Lys43 N	2.91
O4	Ser44 N	2.94
	Ser44 O^{γ}	3.10
	Ow1	2.74
Ow1	Asp140 $O^{\delta1}$	2.98
Ow2	Met45 N	3.22

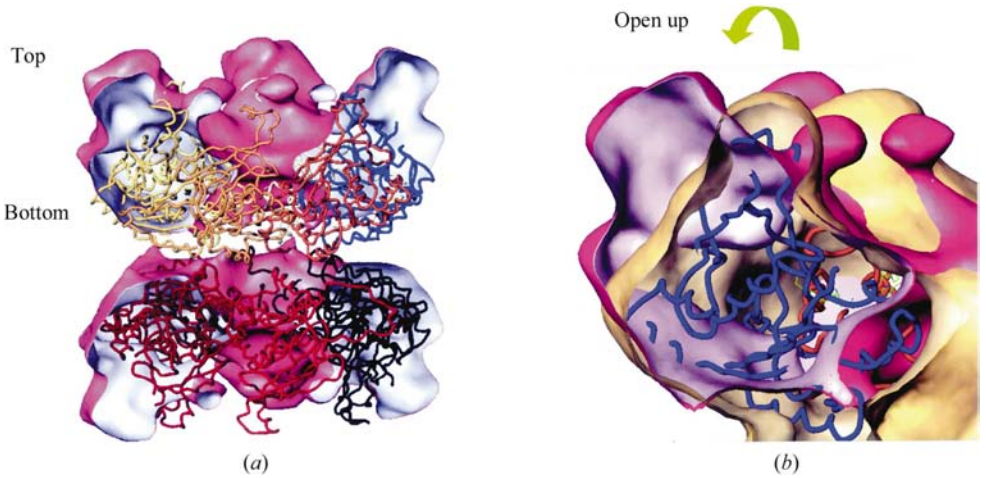

Figure 5
Electron-microscopic studies of RepA in the presence of ATPγS. (*a*) Comparison of the images observed by EM studies in the presence of ATPγS (red surface) and the structure of unliganded RepA at pH 6.0 (wire model; Niedenzu *et al.*, 2001). (*b*) Detailed view of main structural differences found at the 'top' part of RepA. The red outline refers to the image observed by EM studies in the presence of ATPγS; the yellow outline refers to the structure of unliganded RepA at pH 6.0. Electron-microscopy measurements and three-dimensional reconstruction are described in §2.

located after ATP hydrolysis. Biochemical data showed that phosphate does not inhibit ATP binding and hydrolysis, suggesting that phosphate binds to RepA with low affinity. We conclude that the coordination of sulfate to the ATP-binding sites is a consequence of the large excess (200 m*M* $MgSO_4$) of sulfate anions used in the crystallization experiments. All sulfate-anion positions are fully occupied and in the same environment, suggesting that they are identical. For DnaB helicase a small difference is observed in electron-microscopy studies between the hexamer C_6 rings formed in the presence of ADP and those formed in the presence of AMP-PNP. When these two averages are superimposed, it appears that the hole in the centre of the C_6 ring does not change, but that the density of each subunit in the presence of AMP-PNP ring is radially extended by about 5 Å, leading to a ring that is about 10 Å larger in diameter than the ring formed by the DnaB–ADP complex (Yu *et al.*, 1996).

In the present study, conformational changes that lead towards an 'open' stucture of RepA upon binding of nucleotides are both observed by X-ray diffraction and electron microscopy. Since binding of ATP/ADP or analogues to the RepA hexamer is negatively cooperative and three high-affinity and three low-affinity binding sites have been identified, this is probably associated with tertiary structural changes of RepA (Xu, Frank, Niedenzu *et al.*, 2000) that may be of the kind indicated by the above RepA crystal structure and by electron-microscopy studies.

This work was supported by DFG-Sonderforschungsbereich 344, by Fonds der Chemischen Industrie and by European Commission grants BIO4-CT98-0106 and QLK2-CT-2000-00634. We thank R. Diehl for technical assistance, Dr U. Müller (Protein Structure Factory) for help with synchrotron data collection, and T. Maier and A. Meinhart for helpful discussions. We are grateful to Drs E. Lanka and G. Ziegelin for communication of the experimental data prior to publication and to BESSY II (Berlin) for providing X-ray beam time.

References

Böttcher, C., Ludwig, K., Herrmann, A., van Heel, M. & Stark, H. (1999). *FEBS Lett.* **463**, 255–259.
Bowles, J. T. (1998). *Med. Hypotheses*, **51**, 179–221.
Brünger, A. T. (1992). *Nature (London)*, **355**, 472–474.
Brünger, A. T. (1993). *Acta Cryst.* D**49**, 24–36.
Brünger, A. T., Adams, P. D., Clore, G. M., DeLano, W. L., Gros, P., Grosse-Kunstleve, R. W., Jiang, J. S., Kuszewski, J., Nilges, M., Pannu, N. S., Read, R. J., Rice, L. M., Simonson, T. & Warren, G. L. (1998). *Acta Cryst.* D**54**, 905–921.
Egelman, E. H. (1996). *Structure*, **4**, 759–762.
Ellis, N. A. (1997). *Curr. Opin. Genet. Dev.* **7**, 354–363.
Fass, D., Bogden, C. E. & Berger, J. M. (1999). *Structure Fold. Des.* **7**, 691–698.
Heel, M. van & Harauz, G. (1986). *Optik*, **73**, 119–122.
Heel, M. van (1987). *Ultramicroscopy*, **21**, 111–124.
Heel, M. van, Harauz, G., Orlova, E. V., Schmidt, R. & Schatz, M. (1996). *J. Struct. Biol.* **116**, 17–24.
Jones, T. A., Zou, J. Y., Cowan, S. W. & Kjeldgaard, M. (1991). *Acta Cryst.* A**47**, 110–119.
Kim, J. L., Morgenstern, K. A., Griffith, J. P., Dwyer, M. D., Thomson, J. A., Murcko, M. A., Lin, C. & Caron, P. R. (1998). *Structure*, **6**, 89–100.
Korolev, S., Hsieh, J., Gauss, G. H., Lohman, T. M. & Waksman, G. (1997). *Cell*, **90**, 635–647.
Kraulis, P. J. (1991). *J. Appl. Cryst.* **24**, 946–950.
Laskowski, R. A., Moss, D. S. & Thornton, J. M. (1993). *J. Mol. Biol.* **231**, 1049–1067.
Lohman, T. M. & Bjornson, K. P. (1996). *Annu. Rev. Biochem.* **65**, 169–214.
Lukatela, G., Krauss, N., Theis, K., Selmer, T., Gieselmann, V., von Figura, K. & Saenger, W. (1998). *Biochemistry*, **37**, 3654–3664.
Luzzati, V. (1952). *Acta Cryst.* **5**, 802–810.
Matson, S. W. & Kaiser-Rogers, K. A. (1990). *Annu. Rev. Biochem.* **59**, 289–329.
Matthews, B. W. (1968). *J. Mol. Biol.* **33**, 491–496.
Merritt, E. A. & Bacon, D. J. (1997). *Methods Enzymol.* **277**, 505–524.
Navaza, G. (1994). *Acta Cryst.* A**50**, 157–163.
Nichol, L. W. & Roy, A. B. (1966). *Biochemistry*, **5**, 1379–1388.
Nicholls, R. G. & Roy, A. B. (1971). *The Enzymes*, 3rd ed., edited by P. D. Boyer, Vol. 5, pp. 21–41. New York: Academic Press.
Niedenzu, T., Röleke, D., Bains, G., Scherzinger, E. & Saenger, W. (2001). *J. Mol. Biol.* **306**, 479–487.
Notarnicola, S. M., Mulcahy, H. L., Lee, J. & Richardson, C. C. (1997). *J. Biol. Chem.* **272**, 18425–18433.
Orlova, E. V., Dube, P., Harris, J. R., Beckmann, E., Zemlin, F., Markl, J. & van Heel, M. (1997). *J. Mol. Biol.* **271**, 417–437.
Otwinowski, Z. & Minor, W. (1997). *Methods Enzymol.* **276**, 307–326.
Patel, S. S. & Picha, K. M. (2000). *Rev. Biochem.* **69**, 651–697.
Röleke, D., Hoier, H., Bartsch, C., Umbach, P., Scherzinger, E., Lurz, R. & Saenger, W. (1997). *Acta Cryst.* D**53**, 213–216.
Saraste, M., Sibbald, P. R. & Wittinghofer, A. (1990). *Trends Biochem. Sci.* **11**, 430–434.
Sawaya, M. R., Guo, S., Tabor, S., Richardson, C. C. & Ellenberger, T. (1999). *Cell*, **99**, 167–177.
Scherzinger, E., Haring, V., Lurz, R. & Otto, S. (1991). *Nucleic Acids Res.* **19**, 1203–1211.
Scherzinger, E., Ziegelin, G., Barcena, M., Carazo, J. M., Lurz, R. & Lanka, E. (1997). *J. Biol. Chem.* **272**, 30228–30236.
Scholz, P., Haring, V., Wittman-Liebold, B., Ashman, K., Bagdasarian, M. & Scherzinger, E. (1989). *Gene*, **75**, 271–288.
Singleton, M. R., Sawaya, M. R., Ellenberger, T. & Wigley, D. B. (2000). *Cell*, **101**, 589–600.
Soultanas, P. & Wigley, D. B. (2000). *Curr. Opin. Struct. Biol.* **10**, 124–128.
Vagedes, P., Saenger, W. & Knapp, E. W. (2002). *Biophys. J.* **83**, 3066–3078.
Velankar, S. S., Soultanas, P., Dillingham, M. S., Subramanya, H. S. & Wigley, D. B. (1999). *Cell*, **97**, 75–84.
Xu, H., Frank, J., Holzwarth, J. F., Saenger, W. & Behlke, J. (2000). *FEBS Lett.* **482**, 180–184.
Xu, H., Frank, J., Niedenzu, T. & Saenger, W. (2000). *Biochemistry*, **39**, 12225–12233.
Xu, H., Frank, J., Trier, U., Hammer, S., Schröder, W., Behlke, J., Schäfer-Korting, M., Holzwarth, J. F. & Saenger, W. (2001). *Biochemistry*, **40**, 7211–7218.
Yu, X., Jezewska, M. J., Bujalowski, W. & Egelman, E. H. (1996). *J. Mol. Biol.* **259**, 7–14.